Scientific paper

Novel Mannich Bases Based on Schiff Bases: Synthesis, Biological Activities, Computational Approach, and Anticancer Analysis with Molecular Docking

Gül Kotan^{1,*} ©, Kenan Gören² ©, Sevda Manap² ©, Mehmet Bağlan² ©, Haydar Yüksek² ©

1* Department of Chemistry and Chemical Processing Technologies, Vocational School, Kafkas University, Kars, Turkey,

² Department of Chemistry, Faculty of Science and Letters, Kafkas University, Kars, Turkey

* Corresponding author: E-mail: gulkemer@hotmail.com

Received: 04-18-2025

Abstract

In this study, the Mannich base derivatives 1-(2,6-dimethylmorpholin-4-yl-methyl)-3-alkyl(aryl)-4-(3-methoxy-4-acetoxybenzylideneamino)-4,5-dihydro-1*H*-1,2,4-triazole-5-one **6(a-g)** have been synthesized. The spectral analysis of the new compounds were identified utilizing ¹H NMR, ¹³C NMR and IR spectrometry. Three techniques (Blois, Oyaizu, Dinis) were used to assess the potential antioxidant activities of the compound. Using the agar well diffusion method, the compounds' in vitro antibacterial properties were studied against six bacteria. Additionally, the molecular docking study was performed to researh the potential anticancer activities of the compound against ovarian and gastric cancer. In molecular docking analysis, compound **6e** gave good results in potential cancer interactions with protein 3W2S and compound **6f** with protein 3OCB. Also, ADME estimations was performed to assess the drug-likeness of Mannich bases. The energies of molecular orbitals (HOMO-LUMO) and energy differ (ΔEg) was calculated for compounds. Finally, the structure-activity relationships (SAR) was analysized by Density Functional Theory (DFT).

Keywords: 1,2,4-triazol-5-one; Mannich base; Molecular Docking, ADME; DFT; SAR

1. Introduction

Schiff bases are important ligands known for their ability to form stable complexes, their ease of synthesis, and their structural diversity. This versatility is largely due to the presence of nitrogen, sulfur, and oxygen atoms that act as donor sites, endowing Schiff bases and their metal complexes with significant biological activities.² Central to these activities is the azomethine group, a key functional moiety involved in many biological processes.³ As a result, Schiff bases and their complexes have been widely studied for their broad range of pharmacological properties, including antibacterial, analgesic, antioxidant, antimalarial, anti-inflammatory, anticonvulsant, and enzyme inhibitory effects.⁴⁻⁶ Beyond their biological importance, metal complexes of Schiff bases have found valuable applications in fields such as medicine, food chemistry, agriculture, and biochemistry, where they often serve as active catalytic sites.7

In line with these interests, one of the major goals in medicinal and organic chemistry is to design and synthesize molecules with enhanced therapeutic effects.⁸ This need has become more urgent due to the rapid development of resistance against current antimicrobial agents, which limits treatment options and highlights the demand for novel, effective drugs. 9,10 Mannich bases, synthesized through amino alkylation of aromatic substrates, have emerged as promising candidates in this regard. The Mannich reaction introduces aminoalkyl groups that can be further modified, making it a powerful tool for generating biologically active molecules. 11,12 Consequently, Mannich bases exhibit diverse pharmacological properties such as antibacterial, analgesic, anti-inflammatory, anticancer, and anesthetic activities, underscoring their pharmaceutical relevance. 13-15

Another important aspect linked to these bioactivities is the role of free radicals highly reactive molecules containing unpaired electrons which are implicated in

many chronic degenerative diseases including cancer, autoimmune disorders, inflammation, and cardiovascular and neurological diseases. ^{16,17} These radicals are produced naturally during biological processes such as phagocytosis and cell signaling, but when uncontrolled, they damage essential biomolecules like lipids, proteins, and DNA, leading to oxidative stress and tissue injury. ¹⁸ Antioxidants, either endogenous or introduced through diet, mitigate this damage by neutralizing free radicals and thus protect cellular integrity. ¹⁹

Given the wide impact of oxidative stress and the global burden of diseases like cancer, which encompasses over 100 different types affecting various organs, ongoing research to develop effective treatments is crucial.^{20,21} For instance, ovarian cancer is among the most common and deadly cancers in women worldwide ^{22,23}, while stomach cancer ranks highly in global cancer incidence and mortality rates.²⁴ These facts emphasize the importance of discovering new anticancer agents

Motivated by these challenges, the present study focuses on the synthesis of novel Mannich bases, their structural characterization by 13C NMR, 1H NMR, and IR spectroscopy, and the evaluation of their antimicrobial and antioxidant properties using Dinis²⁵, Blois²⁶, and Oyaizu²⁷ assays. To complement the experimental work, Density Functional Theory (DFT) calculations were performed to elucidate electronic and structural properties of the compounds, bridging theory with experiment. 28,29 Additionally, drug-likeness was assessed via ADME analysis, and molecular docking studies investigated the potential anticancer activity of the synthesized compounds against ovarian and stomach cancer targets. The relationship between molecular properties such as HOMO-LUMO energies, molecular weight, total energy, and volume and antibacterial activity was also explored to understand SAR (structure-activity relationship).

The free radical scavenging capacity of 1,2,4-triazole derivatives and reported that these compounds possess strong antioxidant properties.³⁰ The high anti-inflammatory and radical scavenging activity of the 6b derivative was particularly noteworthy. Mannich bases con-2,6-dimethylmorpholine exhibited antioxidant activity in DPPH and metal ion chelation tests and effective antibacterial properties against both Gram-positive and Gram-negative bacteria.31 The 1,2,4-triazole derivatives are effective against important pathogens such as Staphylococcus aureus and Escherichia coli.32 The synthesis, characterization, antioxidant and antimicrobial activities of 1,2,4-triazole derivatives containing 2,6-dimethylmorpholine using various methods were studied.³³ The acetylcholinesterase and glutathione S-transferase enzyme inhibitory activity of new Mannich bases both in vitro and in-silico was evaluated. These results indicate that these Mannich bases hold promise in biomedical applications due to their antioxidant and antibacterial activities.34

2. Experimental

2. 1. Materials and Reagents

The chemical reagents used in this investigation were acquired from Fluka, Aldrich, and Merck AG. Melting points were determined using the Stuart SMP30 instrument. Infrared spectrum data were recorded with Alpha-P Bruker FT-IR spectrometer. ¹³C and ¹H NMR spectra were taken with the Bruker Avance III spectrometer. PG Devices Ltd T80 UV/VIS instrument was used to measure the synthesized compounds' antioxidant properties. Graphs measuring antioxidant activity were done utilizing the Microsoft Excel 97-2003 application. The synthesized compounds' synthesis scheme was drawn with the ChemDraw 22 program. Molecular docking analysis used to evaluate the synthesized compounds as potential drug candidates was utilized Schrödinger's Maestro Molecular Modeling program³⁵ and ADME analysis was performed using online websites like SwissADME.³⁶ The Gaussian09 program was used for SAR analysis.³⁷

2. 2. Synthesis

Acetic anhydride (2) and 4-hydroxy-3-methoxy-benzaldehyde (1) reacted to yield the chemical 4-formyl-2-methoxyphenyl acetate (3) in this investigation. As a result of the reaction of 4-formyl-2-methoxyphenyl acetate with 3-alkyl(aryl)-4-amino-4,5-dihydro-1*H*-1,2,4-triazol-5-one (4a-g) compounds Schiff bases 5(a-g) have been synthesized.³⁸ The 6(a-g) compound have been synthesized by the reaction of 5(a-g) Schiffs with 2,6-dimethylmorpholine in the presence of formaldehyde considering the Mannich reaction and visualized in the Scheme 1.³⁴

2. 2. 1. General Procedure for Synthesis of 1-(2,6-dimethylmorpholin-4-ylmethyl)-3-alkyl(aryl)-4-(4-formyl-2-methoxyphenylacetoxybenzylideneamino)-4,5-dihydro-1*H*-1,2,4-triazole-5-one 6(a-g)

0.01 mol of the 5(a-g) compounds was dissolved in 0.1 L of ethanol. Then, 0.010 mol of 2,6-dimethyl morpholine and 0.03 mol of formaldehyde (35%) solution were added. The mixture was stirred for 3 hours and subsequently stored at $-16\,^{\circ}\text{C}$ in a deep freezer to induce precipitation. The crude precipitate was collected by filtration, washed with cold ethanol, and crystallized several times. Finally, the crystals were vacuumdried and identified as compounds 6(a-g).

6a: mp 111 °C, yield 88%, IR: 1765, 1705 (C=O), 1599 (C=N), 1262 (COO), 862 and 836 (1,2,4-trisubstituted benzenoid ring) cm⁻¹; ¹H NMR (DMSO- d_6 , δ): 1.03–1.13 (m, 6H, 2CH₃), [2.20 (t, J = 10.80 Hz), 2.29–2.33 (m), 2.65 (m), 2.76 (d, J = 10.4 Hz), 3.51–3.55 (m), 3.84–3.87

(m)] (Morpholine H), 2.29 (s, 3H, COCH₃), 2.33 (s, 3H, CH₃), 3.85 (s, 3H, OCH₃), 4.55 (s, 2H, NCH₂N), 7.23 (d, 1H, Ar-H; J = 8.00 Hz), 7.47 (dd, 1H, Ar-H; J = 8.40, 1.60 Hz), 7.90 (d, 1H, Ar-H; J = 2.00 Hz), 9.70 (s, 1H, N=CH); 13 C NMR (DMSO- d_6 , δ): 10.96 (CH₃), 17.89, 18.92 (2CH₃), 20.37 (COCH₃), [55.01 (CH₂), 55.59 (CH₂), 71.03 (2CH)] (Morpholine C), 55.96 (OCH₃), [65.40, 65.62, 66.23] (NCH₂N), [111.56 (CH), 120.56 (CH), 123.48 (CH), 132.24 (C), 141.87 (C), 151.29 (C)] (ArC), 143.12 (Triazol C₃), 150.23 (Triazol C₅), 153.55 (N=CH), 168.26 (COCH₃).

6b: mp 119 °C, yield 86%, IR: 1763, 1695 (C=O), 1581 (C=N), 1271 (COO), 865 and 809 (1,2,4-trisubstituted benzenoid ring) cm⁻¹; ¹H-NMR (DMSO- d_6 , δ): 0.97 (t, 3H, CH₂CH₂CH₃; J = 7.20 Hz), [2.01 (t, J = 10.80 Hz), 2.27–2.29 (m), 2.68–2.70 (m), 2.77 (d; J = 10.40 Hz), 3.53 (m)] (Morpholine H), 2.29 (s, 3H, COCH₃), 2.70 (t, 2H, CH₂CH₂CH₃; J = 7.20 Hz), 3.85 (s, 3H, OCH₃), 4.57 (s, 2H, NCH₂N), 7.24 (d, 1H, Ar-H; J = 8.00 Hz), 7.47 (dd, 1H, Ar-H; J = 8.00, 1.60 Hz), 7.59 (d, 1H; Ar-H; J = 1.60 Hz), 9.69 (s, 1H, N=CH); ¹³C NMR (DMSO- d_6 , δ): 13.36 (CH₂CH₂CH₃), 17.89, 18.93 (2CH₃), 18.97 (CH₂CH₂CH₃), 20.37 (COCH₃), 26.51 (CH₂CH₂CH₃), [55.04 (CH₂), 55.64 (CH₂), 71.02 (2CH)] (Morpholine C), 55.93 (OCH₃), [65.40, 65.62, 66.20] (NCH₂N), [111.65 (CH), 120.41 (CH), 123.54 (CH), 132.27 (C), 141.86 (C), 151.29 (C)]

(ArC), 145.64 (Triazol C_3), 150.29 (Triazol C_5), 153.60 (N=CH), 168.67 (\underline{C} OCH₃).

6c: mp 137 °C, Yield 85%, IR: 1759, 1713 (C=O), 1584 (C=N), 1294 (COO), 884 and 835 (1,2,4-trisubstituted benzenoid ring), 753 and 701 (monosubstituted benzenoid ring) cm⁻¹; ¹H NMR (DMSO- d_6 , δ): [1.04 (d; J = 6.40Hz), 1.12 (d; J = 6.40 Hz)] (6H, 2CH₃), [2.02 (t, <math>J = 10.80Hz), 2.28-2.31 (m), 2.67-2.69 (m), 2.79 (d, J = 10.80), 3.52–3.56 (m), 3.84 (m, 3H, OCH₃), 4.11 (s, 2H, CH₂Ph), 4.60 (s, 2H, NCH₂N), 7.22 (d, 1H, ArH; J = 8.00 Hz), 7.21, 7.25 (m, 1H, ArH), 7.30, 7.41 (m, 5H, ArH), 9.65 (s, 1H, N=CH); 13 C NMR (DMSO- d_6 , δ): [17.89, 18.93] (2CH₃), 20.37 (COCH₃), 31.00 (CH₂Ph), [55.06 (CH₂), 55.66 (CH₂), 71.02 (2CH)] (Morpholine C), 55.93 (OCH₃), [65.41, 65.77, 66.35] (NCH₂N), [111.78 (CH), 121.13 (CH), 123.47 (CH), 132.21 (C), 141.90 (C), 151.27 (C)] (ArC), [126.79 (CH), 128.49 (2CH), 128.61 (2CH), 135.76 (C)] (ArC bonded C-3), 144.90 (Triazol C₃), 150.25 (Triazol C₅), 153.00 (N=CH), 168.27 (COCH₃).

6d: mp 128 °C, Yield 76%, IR: 1760, 1694 (C=O), 1597 (C=N), 1271 (COO), 864 and 834 (1,2,4-trisubstituted benzenoid ring), 803 (1,4-disubstituted benzenoid ring) cm⁻¹; ¹H NMR (DMSO- d_6 , δ): [1.04 (d; J = 6.00 Hz), 1.12 (d; J = 6.40 Hz)] (6H, 2CH₃), [2.02 (t, J = 10.80 Hz), 2.29–2.31 (m), 2.67–2.69 (m), 2.79 (d, J = 10.40 Hz), 3.52–

Scheme 1. Synthesis pathway of 6(a-g) compounds.

3.55 (m), 3.85, 3.88 (m)] (Morpholine H), 2.24 (s, 3H, PhCH₃), 2.29 (s, 3H, COCH₃), 3.85 (s, 3H, OCH₃), 4.05 (s, 2H, CH₂Ph), 4.59 (s, 2H, NCH₂N), 7.12 (d, 2H, ArH; J = 8.00 Hz), 7.22 (d, 1H, ArH; J = 8.00 Hz), 7.23 (d, 2H, ArH; J = 8.00 Hz), 7.40 (dd, 1H, Ar-H; J = 8.00, 2.00 Hz), 7.51 (d, 1H, ArH; J = 2.00 Hz), 9.64 (s, 1H, N=CH); ¹³C NMR (DMSO- d_6 , δ): [17.89, 18.93] (2CH₃), 20.38 (COCH₃, 20.56 (PhCH₃) 30.61 (CH₂Ph), [55.07 (CH₂), 55.67 (CH₂), 71.01 (2CH)] (Morpholine C), 55.91 (OCH₃), [65.41, 65.74, 66.32] (NCH₂N), [110.77 (CH), 121.14 (CH), 123.47 (CH), 132.23 (C), 141.89 (C), 151.27 (C)] ArC, [128.53 (2CH), 129.06 (2CH), 132.62 (C), 135.90 (C)] (ArC bonded C-3), 145.05 (Triazol C₃), 150.25 (Triazol C₅), 152.93 (N=CH), 168.28 (COCH₃).

6e: mp 126 °C, Yield 73%, IR: 1755, 1710 (C=O), 1584 (C=N), 1296 (COO), 904 and 829 (1,2,4-trisubstituted benzenoid ring), 829 (1,4-disubstituted benzenoid ring) cm⁻¹; ¹H NMR (DMSO- d_6 , δ): [1.04 (d; J = 6.40 Hz), 1.12 (d; J = 6.40 Hz)] (6H, 2CH₃), [2.02 (t, J = 10.80 Hz), 2.28-2.30 (m), 2.67-2.70 (m), 2.79 (d, J = 10.40 Hz), 3.52-3.56 (m), 3.84-3.88 (m)] (Morpholine H), 2.29 (s, 3H, COCH₃), 3.70 (s, 3H, OCH₃), 4.04 (s, 2H, CH₂Ph), 4.59 (s, 2H, NCH₂N), 6.88 (d, 2H, ArH; J = 8.80 Hz), 7.23 (d, 2H, ArH; J = 8.40 Hz), 7.26 (d, 1H, ArH; J = 8.40 Hz), 7.42 (dd, 1H, ArH; J = 8.00, 1.60 Hz,), 7.53 (d, 1H, ArH; J = 1.60Hz), 9.65 (s, 1H, N=CH); 13 C NMR (DMSO- d_6 , δ): [17.88, 18.73] 2CH₃, 20.37 (COCH₃), 30.14 (CH₂Ph), [55.02 (CH₂), 55.66 (CH₂), 71.02 (2CH)] (Morpholine C), 55.07 (OCH_3-p) 55.93 (OCH_3) , [65.41, 65.75, 66.33] (NCH_2N) , [110.85 (CH), 121.09 (CH), 123.48 (CH), 132.24 (C), 141.89, 151.28 (C)] (ArC), [113.93 (2CH), 127.48 (C), 129.72 (2CH), 158.15 (C)] (ArC bonded C-3), 145.21 (Triazol C₃), 150.26 (Triazol C₅), 153.00 (N=CH), 168.28 (COCH₃).

6f: mp 124 °C, Yield 79%, IR: 1763, 1695 (C=O), 1578 (C=N), 1273 (COO), 834 and 863 (1,2,4-trisubstituted benzenoid ring), 800 (1,4-disubstituted benzenoid ring) cm⁻¹; ¹H NMR (DMSO- d_6 , δ): [1.03 (d; J= 6,00 Hz), 1.12 (d; J = 6.40 Hz)] (6H, 2CH₃), [2.02 (t, J = 10.80 Hz), 2.29-2.32 (m), 2.63-2.86 (m), 2.78 (d, J = 10.00 Hz), 3.51-3.56 (m), 3.83-3.85 (m)] (Morpholine H), 2.29 (s, 3H, COCH₃), 3.89 (s, 3H, OCH₃), 4.13 (s, 2H, CH₂Ph), 4.59 (s, 2H, NCH₂N), 7.22 (d, 1H, ArH; J = 8.00 Hz), 7.38–7.41 (m, 5H, ArH), 7.50 (d, 1H, ArH; J = 1.60 Hz,) 9.66 (s, 1H, N=CH); 13 C NMR (DMSO- d_6 , δ): [17.90, 18.94] (2CH₃), 20.39 (COCH₃), 30.33 (CH₂Ph), [55.05 (CH₂), 55.65 (CH₂), 71.03 (2CH)] (Morpholine C), 55.95 (OCH₃), [65.42, 65.81, 66.40] (NCH₂N), 110.87 (CH), 121.13 (CH), 123.50 (CH), 132.17 (C), 141.95 (C), 151.30 (C)] (ArC), [128.45 (2CH), 130.59 (2CH), 131.51 (C), 134.78 (C)] (ArC bonded C-3), 144.60 (Triazol C₃), 150.26 (Triazol C_5), 153.16 (N=CH), 168.29 (COCH₃).

6g: mp 179 °C, Yield 85%, IR: 1765 and 1695 (C=O), 1584 (C=N), 1273 (COO), 864 and 838 (1,2,4-trisubstituted benzenoid ring), 750 and 693 (monosubstituted benzenoid ring) cm⁻¹; ¹H NMR (DMSO- d_6 , δ): [1.05 (d; J = 6.40

Hz), 1.14 (d; J = 6.40 Hz)] (6H, 2CH₃), [2.10 (t, J = 10.80 Hz), 2.30–2.32 (m), 2.66-2.69 (m), 2.84 (d, J = 10.40 Hz), 3.54–3.57 (m), 3.82 (m)] (Morpholine H), 2.29 (s, 3H, COCH₃), 3.81 (s, 3H, OCH₃), 4.71 (s, 2H, NCH₂N), 7.25 (d, 1H, ArH; J = 8.00 Hz), 7.45 (dd, 1H, ArH; J = 8.00, 1.60 Hz), 7.55–7.58 (m, 4H, ArH), 7.91–7.94 (m, 2H, ArH), 9.65 (s, 1H, N=CH); ¹³C NMR (DMSO- d_6 , δ): [17.89, 18.93] (2CH₃), 20.37 (COCH₃), [54.99 (CH₂), 55.56 (CH₂), 71.08 (2CH)] (Morpholine C), 55.86 (OCH₃), [65.43, 66.17, 66.78] (NCH₂N), 111.46 (CH), 120.93 (CH), 123.61 (CH), 132.11 (C), 142.05 (C), 151.30 (C)] (ArC), [126.12 (C), 128.20 (2CH), 128.56 (2CH), 130.36 (CH)] (ArC bonded C-3), 144.60 (Triazol C₃), 150.26 (Triazol C₅), 153.16 (N=CH), 168.29 (COCH₃).

2. 3. Antioxidant Activity

2. 3. 1. Reducing Power

The reducing power of the synthesized compounds was determined using the Oyaizu technique.²⁷ The premise behind this method is that the reducing agent in the extracts converts Fe³ ions to Fe² ions, and that the addition of FeCl₂ creates the Prussian blue hue. A compound's reducing capacity can be a useful predictor of its potential antioxidant activity.³⁹ Various mechanisms have been associated with antioxidant activity, including inhibition of chain initiation, binding of transition metal ion catalysts, breakdown of peroxides, suppression of hydrogen evolution, radical scavenging, and reducing power. The high absorbance value indicates high reducing power.⁴⁰ For each synthesized compound, 100, 250, 500 μg\mL concentrations were prepared and 1 mL from each was taken. For 20 minutes, the resulting mixture was maintained at 50 °C. After incubation, 1 mL of the sample was mixed with 1 mL of purified water and 0.2 mL of 1% FeCl₃ solution. The absorbance of the resulting solution was measured at 700 nm. As control agents, BHT, BHA, and α-tocopherol were employed.

2. 3. 2. Radical Scavenging Activity

An example of a stable organic radical is 1,1-diphenyl-2-picrylhydrazyl (DPPH). The antioxidant capacity of biological reagents can be used to assess their potential to scavenge DPPH radicals. DPPH oxidative assay is used worldwide to measure radical scavenging capacity. Blois' method was used to determine the DPPH radical scavenging effect. According to this method, as the electron-donating ability of the extracts increases, the purple color of the DPPH radical fades and the measured absorbance decreases. Concentrations of 12.5, 25, and 37.5 μ g/mL were prepared from each sample and 1 mL of each of these concentrations was added to 4 mL of 0.1 mM DPPH. After 30 minutes of darkness, the absorbance values at 517 nm were determined. Three replicates were run for each sample. BHT, α -tocopherol and BHA were utilized as control rea-

gents. The absorbance values of the samples were compared with the control, and the following formula was used to calculate the radical scavenging activity (% inhibition).

2. 3. 3. Metal chelate Activity

The chelation of transition metals is one of the mechanisms of antioxidative activity, which stops Fenton-type reactions and hydroperoxide breakdown from being catalyzed. The metal chelating ability of the synthetic compounds was determined using the technique established by Dinis et al.²⁵ Samples and standards were diluted with pure water in test tubes to prepare concentrations of 30, 45, and 60 μ g/mL with a total volume of 200 μ L. 0.05 mL of 2 mM FeCl₂·4H₂O and 0.35 mL of pure water were added. Distilled ethanol was added to make the final volume 4 mL, 0.2 mL of 5 mM ferrozine solution was added to start the reaction. After mixing, the mixture was left for 10 minutes at room temperature. Following incubation, the solution's absorbance at 562 nm was measured and compared to the blank, which was made up of all the solution except the sample. The control was prepared using pure water instead of the sample solutions. The results were given as %Fe²⁺ ion chelating capacity. The spectrophotometric measurement in this investigation depends on the production of a dark purple complex with ferrozine and FeCl₂. Since iron ions chelated by antioxidant substances cannot bind to ferrozine, the intensity of the purple color formed is reduced, resulting in a lower absorbance. A low absorbance value indicates a high chelating capacity.

2. 4. Antimicrobial Activity

In our research, we used the agar well diffusion method to assess the antibacterial properties of the synthesized compounds. This technique, similar to the disk diffusion method, is commonly used to evaluate antibacterial activity against various bacterial strains. 43 The target bacteria were uniformly spread on agar plates. Wells were then punched into the agar using a sterile cork borer, and the synthesized compounds were added into these wells. Following incubation, the antibacterial activity was evaluated by measuring the inhibition zones formed around the wells. The inhibition zones were measured with a ruler after the novel compounds were added to the Petri dishes. The antimicrobial efficacy of the compounds was then compared to that of standard antibiotics. Thus, the antimicrobial results of the compounds were obtained and compared with standard antibiotics. The produced compounds' antibacterial efficacy against the references (Ampicillin, Streptomycin and Neomycin) and six distinct bacteria (Bacillus subtilis (A), Bacillius cereus (B), Pseudomonas aeruginosa (C), Klebsiella pneumoniae (D), Staphylococcus aureus (E), Esherichia coli (F) the antibacterial activity effects have been visually presented in Figure 1, 2.

2. 5. DFT Study

The use of DFT calculations in large-scale quantum chemistry on multielectronic systems and the development of concepts regarding inhomogeneous fluids and phase transitions is another major area where DFT calculations are advancing. DFT calculations have been a valua-

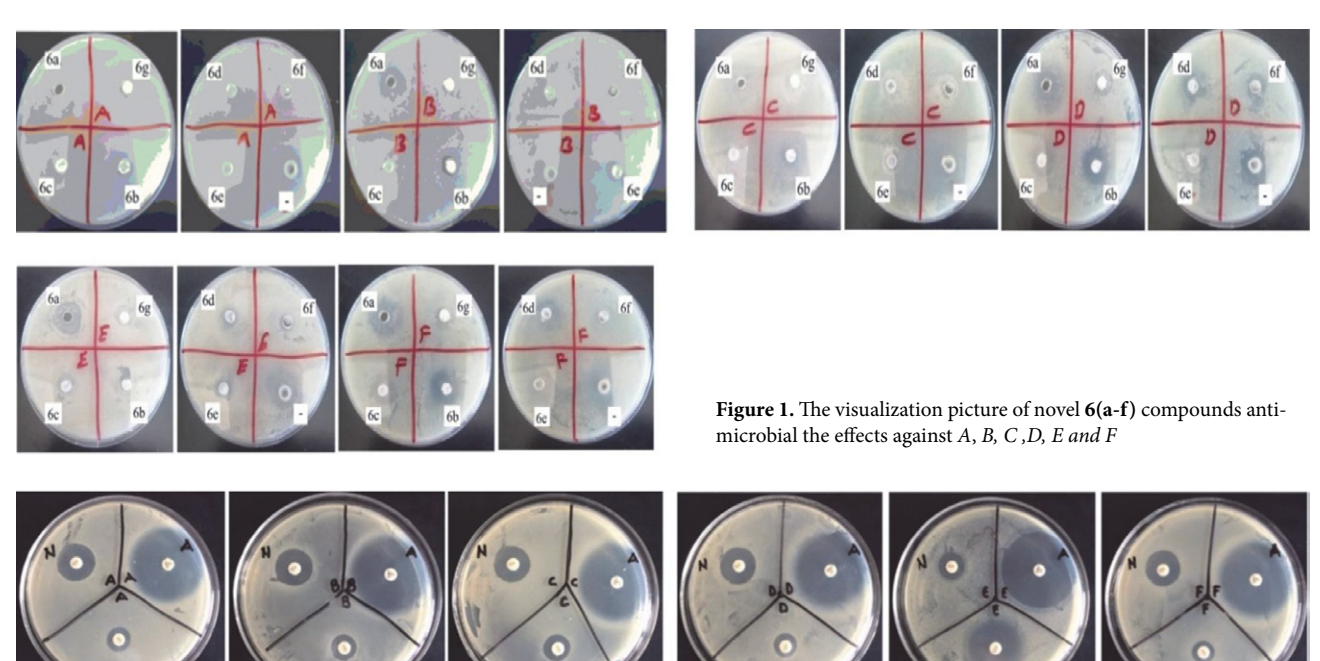


Figure 2. The visualization picture of Ampicillin, Streptomycin and Neomycin antimicrobial effects against A, B C, D, E and F.

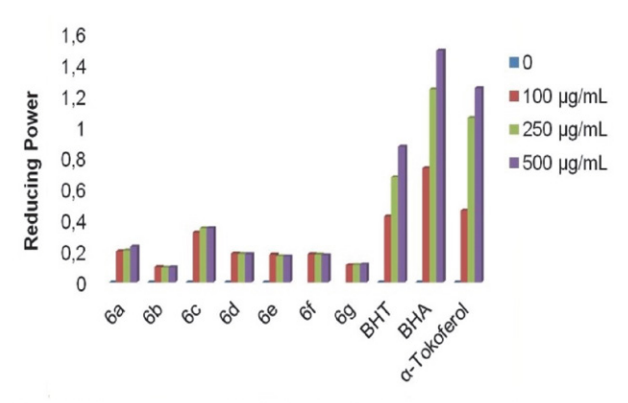
ble research tool for many applications.⁴⁴ Structure-activity relationships (SAR) use specific quantum descriptors such as E_{LUMO}, E_{HOMO}, dipole moment, energy gap, volume, total energy, global stiffness, and molecular polarizability to provide an accurate link to biological activity. DFT calculations provide information on energy functionals, as well as electric, spin, magnetic, catalytic, intermolecular, and chemical reactivity properties.⁴⁵ Geometry optimizations of the synthesized compounds were performed using the B3LYP⁴⁶ hybrid functional with the 6-311G(d,p) basis set, implemented in the Gaussian 09 program.³⁷ The main purpose of the DFT calculations in this study was to obtain theoretical LUMO values, total energy, and volume for SAR (structure-activity relationship) analysis, and to compare these results with antimicrobial activity data.

3. Results and Discussion

3. 1. Antioxidant Activity

3. 1. 1. Reducing Power

The reducing powers of the synthesized compounds were determined according to the Oyaizu method and compared with the values of standard antioxidants. The absorbance values measured at 700 nm in the UV spectrophotometer are given in Table S1. In order to compare the reducing powers of the compounds, the values given in Table S1 were used and are given graphically in Figure 3. According to the data in Figure 3, it was observed that the absorbance values of the compounds were very low compared to the standards and that the synthesized compounds did not show reducing properties.



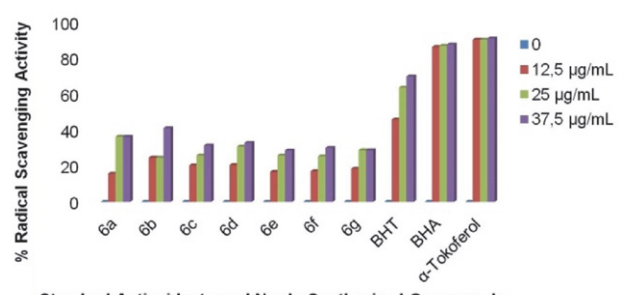
Standard Antioxidants and Newly Synthesized Compounds

Figure 3. The reducing power of standard antioxidants and the 6(a-g) compounds at molar concentrations 0, 100, 250, 500 μg\mL

3.1.2. Radical Scavenging Activity

The results of the radical scavenging activity tests of the novel compounds 6(a-g), along with the reference an-

tioxidant substances (α-tocopherol, BHA, and BHT), are presented in the graph below (Figure 4, Table S2). In the graph, the radical scavenging activities of the synthesized compounds, measured at 517 nm across various concentrations, are expressed as percentage inhibition. According to the data, the activities of compounds **6c**, **6d**, **6e**, and **6f** increased with concentration, whereas compounds **6a**, **6b**, and **6g** showed no concentration-dependent change. Additionally, the radical scavenging activities of all synthesized compounds **6(a-g)** were found to be lower than those of the reference antioxidants.

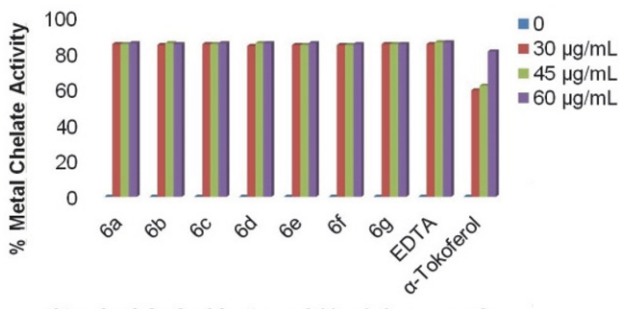


Standard Antioxidants and Newly Synthesized Compounds

Figure 4. The radical scavenging activities of standard antioxidants and the 6(a-g) compounds at molar concentrations 0, 12.5, 25, 37.5 µg\mL

3. 1. 3. Metal Chelate Activation

The percentage inhibition of the synthesized Mannich bases 6(a-g) and the activities of reference antioxidants (α-tocopherol and EDTA) are presented in Figure 5 and Table S3. The metal-chelating ability of phenolic compounds is determined by the presence, position, and number of specific functional groups in their structures. It is known that phenolic compounds containing at least two of the following functional groups -OH, -COOH, -SH, -PO₃H₂, -NR₂, C=O, -O and -S possessing an appropriate structural configuration exhibit enhanced metal-chelating properties.⁴⁷ In this study, the synthesized compounds were found to exhibit strong metal-chelation activity, likely due to the presence of C=O, -NR₂, and -O- groups in their structures. When compared with the reference antioxidants, EDTA displayed similar chelation activity, while α-tocopherol exhibited lower activity.



Standard Antioxidants and 6(a-g) Compounds

Figure 5. The metal chelate activities of standards and the 6(a-g) compounds at molar concentrations 0, 12.5, 25, 37.5 μg/mL

3. 2. Antimicrobial Activity

The antibacterial properties of the newly synthesized compounds **6(a-g)** were evaluated against six different bacterial strains using the agar well diffusion method. *Neomycin, Ampicillin,* and *Streptomycin* were employed as standard antibiotics. Table 1 presents the antimicrobial activity results of both the standards and the synthesized compounds. According to the results, the synthesized compounds exhibited the highest activity against *Klebsiella pneumoniae* and *Escherichia coli,* while the weakest activity was observed against *Pseudomonas aeruginosa.* Among all tested compounds, compound **6a** was the only one that demonstrated activity against all bacterial strains.

tential therapeutic targets in ovarian (PDB ID: 3W2S) and stomach cancer (PDB ID: 3OCB), along with *in silico* study results for these compounds. Molecular docking was performed using the Standard Precision (SP) mode of the Glide module, accessed via the Maestro interface of the Schrödinger software süite.³⁵ This method provides a balanced approach between speed and accuracy when estimating the binding affinities and interaction probabilities of ligands with target proteins. During the docking process, the active sites of the proteins were defined based on the positions of co-crystallized ligands within the crystal structures (PDB IDs: 3W2S and 3OCB) obtained from the Protein Data Bank.⁵³ A grid box was generated to encompass the biologically relevant binding regions of the pro-

Table 1. The zone diameter values against bacteria of synthesized compounds

Compound	(A) Bacillus	(B) Bacillius	(C) Pseudomonas	(D) Klebsiella	(E) Staphylococcus	(F) Escherichia
Code	subtilis	cereus	aeruginosa	pneumoniae	aureus	coli
6a	12 (++)	15 (++)	11 (++)	18 (+++)	18 (+++)	22 (+++)
6b	8 (+)	9 (+)	_	19 (+++)	_	16 (++)
6c	11 (++)	9 (+)	_	14 (++)	_	14 (++)
6d	_	_	_	11 (++)	8 (++)	13 (++)
6e	_	9 (+)	10 (++)	_	8 (++)	12 (++)
6f	_	_	_	10 (++)	8 (++)	_
6g	8 (+)	10 (++)	_	12 (++)		8 (++)
Ampicillin	33	36	36	35	37	34
Streptomycin	17	17	14	16	13	16
Neomycin	12	12	12	11	21	10

[&]quot;The inhibition zone: (-): <5.5 mm; (+): 5.5-10 mm; (++): 11-16 mm; (+++): $\ge 17 \text{ mm}$ "

3. 3. Biochemical Results

3. 3. 1. Molecular Docking Studies

Molecular docking is a crucial technique in modern drug development, enabling the assessment of both the type and strength of molecular interactions with target biomolecules.⁴⁸ Depending on the specific bioactivity of interest, interactions with various targets can be analyzed, allowing for more detailed investigations to be conducted faster and more cost-effectively using data obtained through modern scientific advancements. 49 Research has shown that vascular endothelial growth factor (VEGF) plays a significant role in the proliferation and survival of cancer cells.⁵⁰ One promising approach in anticancer drug design is to inhibit the receptor responsible for the release of VEGF. Targeted or disease-oriented drug development typically involves five phases, the first three of which are commonly conducted through in silico methods.⁵¹ It is widely recognized that biomedical research is both expensive and labor-intensive. To optimize research costs and enhance efficiency, in silico studies are considered indispensable in the early stages of drug discovery.⁵²

This section presents the molecular docking analysis of compounds 6(a-g) with protein structures that are po-

teins, thereby enhancing the realism and reliability of the analysis.

The docking scores obtained from the molecular docking analysis of the novel Mannich bases have been presented in Table 2. Analysis of the data revealed that compounds **6e** and **6f** exhibited the most potent inhibitory activity against the ovarian cancer target (PDB ID: 3W2S; docking score: -9.91) and the gastric cancer target (PDB ID: 3OCB; docking score: -9.91), respectively. Consistent with these findings, ADME analysis indicated that compounds 6e and 6f demonstrated favorable pharmacokinetic properties and compatibility with the docking results. The 3D and 2D interactions of these two compounds with their respective receptors, generated using Discovery Studio 2016, have been illustrated in Figures 6 and 7. According to the literature, the protein targets represented by PDB IDs 3W2S⁵⁴ and 3OCB.⁵⁵ are widely utilized in ovarian and stomach cancer research, respectively. Additionally, favorable docking scores were obtained when evaluating these proteins with their reference ligands. Considering the high binding affinities of compounds **6e** and **6f**, these synthesized compounds show promising preliminary potential for further development as structure-based drug candidates targeting ovarian and stomach cancers in silico.

Compounds			Docking Score		
	(PDB: 3W2S)	Control Ligand	(PDB: 3OCB)	Control Ligand	
6a	-7.06	-9.20	-7.86	-10.30	
6b	-6.05	-9.20	-9.53	-10.30	
6c	-7.90	-9.20	-9.91	-10.30	
6d	-7.70	-9.20	-8.10	-10.30	
6e	-8.10	-9.20	-9.20	-10.30	
6f	-7.50	-9.20	-9.30	-10.30	
6g	-7.40	-9.20	-8.32	-10.30	

Table 2. Binding scores with PDB:3W2S, PDB:3OCB enzymes of 6(a-g) and control ligands

Table 2 presents the docking scores obtained from the molecular docking analysis of the synthesized compound **6e** (docking score: -8.10) and the control ligand, 1-(3-(2-chloro-4-((5-(2-(2-hydroxyethoxy)ethyl)-5H-pyrrolo[3,2-d]pyrimidin-4-yl)amino)phenoxy)phenyl)-3-cyclohexylurea (docking score: -9.20), with the 3W2S protein. The docking scores in Table 2 indicate that the binding affinity of compound **6e** is comparable to that of the natural ligand. Figure 9 illustrates the 2D interaction diagrams of compound **6e** and the control ligand with the 3W2S protein. Upon examining Figure 6, it was observed that the target proteins share similar amino acid residues, except for differences in the receptor binding sites and the

classes of interactions with the ligands, such as π - π T-shaped and π -Anion interactions. Figure 7 depicts both 3D and 2D interaction models of compound **6e** docked with the 3W2S protein, highlighting the amino acids present in the receptor binding sites and the corresponding interaction types with the ligand. Upon examining Figure 7, the amino acids and binding distances seen as a result of the docking analysis are here; conventional hydrogen bonds ARG-841 (5.55 Å) in the oxygen in the triazole ring, LYS-745 (4.83 Å) in the acetoxy part of the compound, VAL-876 (5.41 Å and 6.48) carbon hydrogen bonds in the 2,6-dimethylmorpholine ring, ARG-841 (5.19 Å and 5.24 Å) π -Cation bonds in triazole and benzene ring, PHE-723

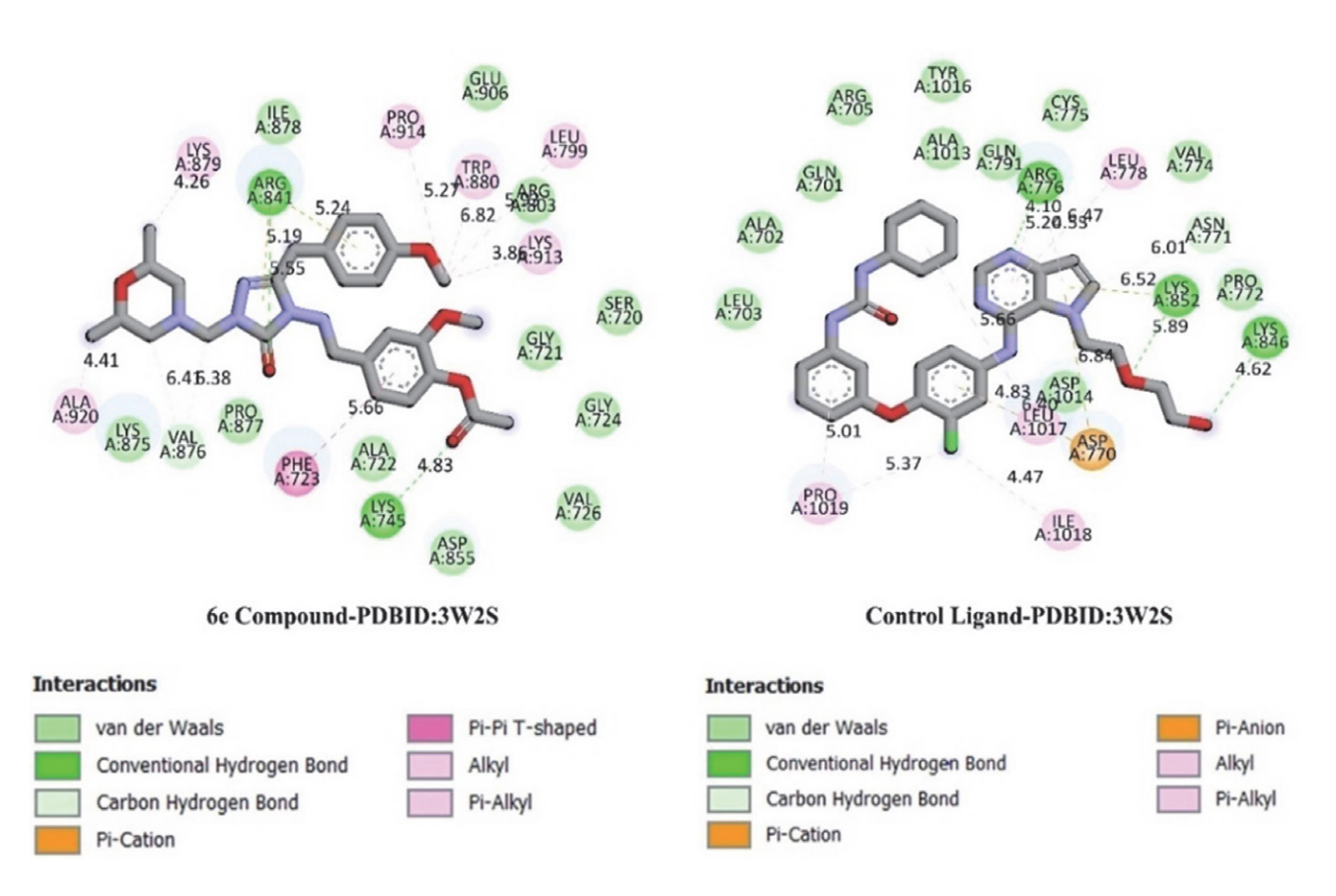


Figure 6. 6e Compound-PDBID:3W2S and control ligand-PDBID:3W2S 2D Mode view

Kotan et al.: Novel Mannich Bases Based on Schiff Bases: Synthesis, ...

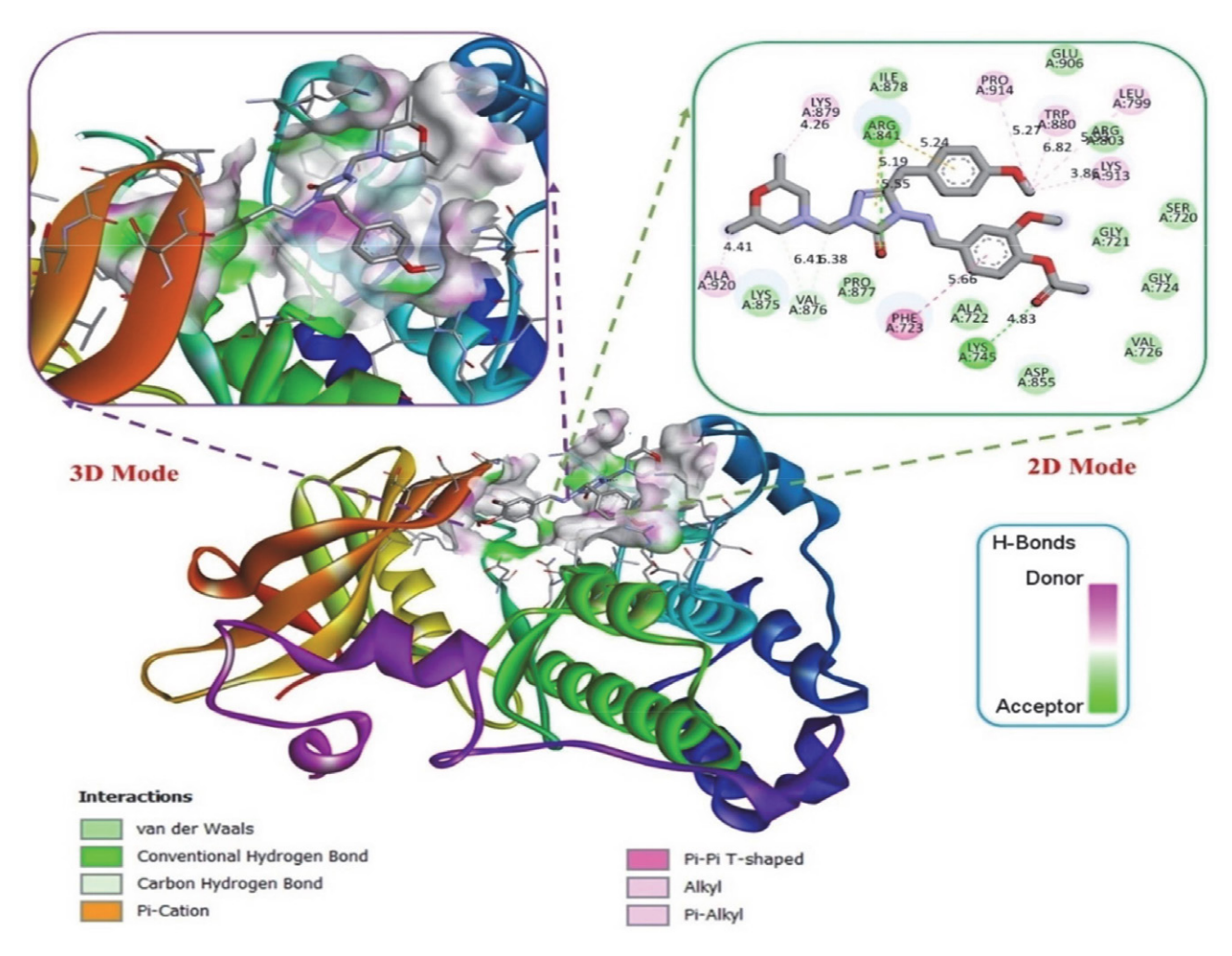


Figure 7. Interacts with 3W2S (Docking Score: -8.10) enzym of synthesized 6e compound; 2D view of ligand-enzyme interactions, 3D view of the donor/acceptor surface of hydrogen bonds on the receptor

 $(5.66 \text{ Å}) \pi - \pi$ T-Shaped bond on the benzene ring of the 3-methoxy-4-acetoxybenzylideneamino group, ALA-920 (4.41 Å), LYS-879 (4.26 Å), PRO-914 (5.27 Å), LEU-729 (5.90 Å), LYS-913 (3.86 Å) Alkyl bonds, TRP-880 (6.82 Å) Pi-Alkyl bond, LYS-875, LYS-875, LYS-875, PRO-877, ASP-875, VAL-726, GLY-724, SER-720 van der Waals bonds.

Table 2 presents the docking scores obtained from the molecular docking analysis of the novel compound $\bf 6f$ (docking score: -9.30) and the control ligand, (2S)-1-(4-(7H-pyrrolo[2,3-d]pyrimidin-4-yl)piperazin-1-yl)-3-amino-2-((4-chlorocyclohexyl)methyl)propan-1-one (docking score: -10.30), with the 3OCB protein. The docking scores indicate that the binding affinity of compound $\bf 6f$ is comparable to that of the natural ligand. Figure 8 shows the 2D interaction diagrams of compound $\bf 6f$ and the control ligand with the 3OCB protein. Upon examination of Figure 8, it was observed that the target proteins share similar amino acid residues, with differences mainly in the receptor binding sites and the types of interactions involved, including π -Cation, π -Donor Hydrogen Bond,

Carbon Hydrogen Bond, and π -Anion interactions. Figure 9 illustrates the 3D and 2D interaction models of compound **6f** docked with the 3OCB protein, highlighting the interacting amino acids and the nature of their chemical interactions. Upon examining Figure 9, the amino acids and binding distances seen as a result of the docking analysis are here: Conventional hydrogen bonds of THR-291 (4.60 Å) to the acetoxy part of compound **6f**, and THR-160 (4.35 Å) to the oxygen in the triazole 2,6-dimethylmorpholine ring, VAL-876 (5.41 Å and 6.48) carbon hydrogen bonds in the triazole and benzene ring, ARG-4 (7.02 Å and 7.20 Å) π -Cation bonds and GLU-234 (6.70 Å and 7.56 Å) π-Anion bond on triazole and benzene ring, VAL-164 (4.92 Å) π -Sigma and MET-227 (5.42 Å) π -Sulfur bonds on the benzene ring of the 3-methoxy-4-acetoxybenzylideneamino group, MET-281 (6.17 Å), ALA-177 (5.18 Å), LEU-156 (4.55 Å), VAL-164 (5.59 Å) Alkyl bonds, PHE-438 (6.41 Å), PHE-161 (5.72 Å) Pi-Alkyl bond, LYS-442, LYS-179, THR-211, TYR-229, ASP-292, ASN-279, PRO-877, ASP-439, GLU-228, and GLY-159 van der Waals bonds.

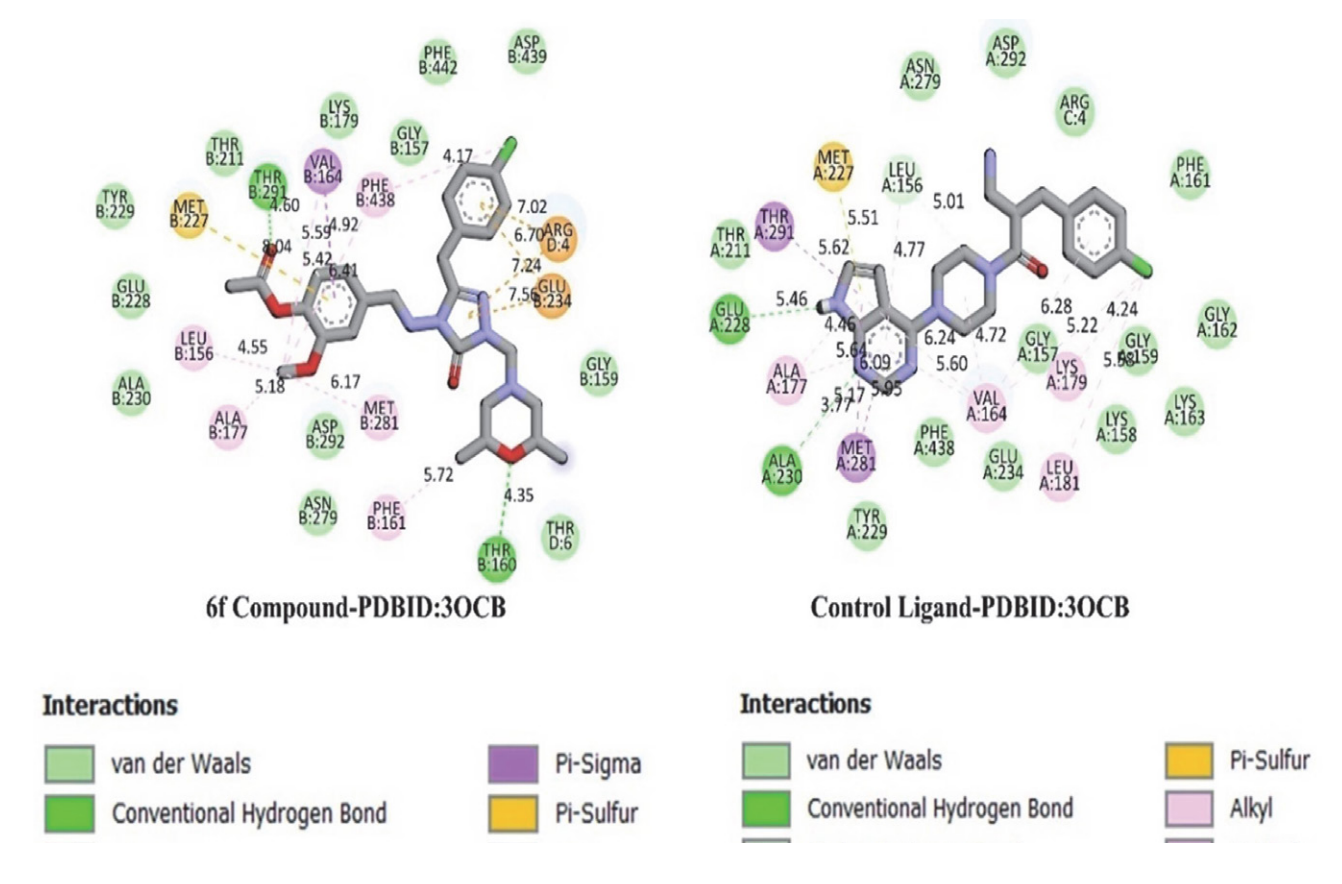


Figure 8. 6f compound-PDBID:3OCB and control ligand-PDBID:3OCB 2D Mode view

3. 3. 2. ADME Analysis

Evaluating the therapeutic potential of a chemical compound primarily involves chemical synthesis, biological screening (both *in vitro* and *in vivo*), and analysis of pharmacokinetic properties. ⁴⁸ Determining pharmacokinetic characteristics such as metabolism, excretion (ADME), and toxicity through *in vivo* studies is a crucial initial step; however, it is an extremely costly process. Therefore, early elimination of poor drug candidates that could lead to clinical failure is essential. SwissADME is a free online platform that offers computational tools to assist in this evaluation. ⁵⁶ It provides valuable information on parameters such as solubility, saturation, lipophilicity, skin permeability, intestinal absorption, and molecular size.

The SwissADME tool was employed to evaluate the drug-likeness potential of the synthesized compounds. These compounds were assessed according to the Lipinski, Veber, and Ghose rules, with the results summarized in Table 3. Compounds that satisfy two or more of these criteria are considered to have high drug-likeness, whereas those meeting fewer than two criteria exhibit lower drug-likeness potential. According to Lipinski's rules, compounds **6a**, **6b**, **6c**, and **6d** comply with all criteria, while compounds **6e** and **6f** violate one rule (molecular weight > 500). Compound **6g** violates two rules (molecular weight > 500 and number of hydrogen bond donors

and acceptors (NorO) > 10). The violation of the molecular weight rule in compounds **6e** and **6f** is likely attributable to the presence of bulky aromatic systems and extended alkyl or heterocyclic side chains, which increase the overall molecular mass and may negatively impact membrane permeability and oral bioavailability. According to Ghose's criteria, compounds 6a and 6d were found to comply with all the rules. However, compound **6b** violated one rule (molar refractivity, MR > 130); compounds 6c, 6e, and 6f violated two rules (molecular weight > 480 and MR > 130); and compound 6g failed to meet three criteria (molecular weight > 480, MR > 130, and total number of atoms > 70). The high molar refractivity in these compounds may result from the presence of multiple π -systems and polarizable atoms (such as halogens or sulfur), which affect the electronic distribution and can influence receptor binding or distribution characteristics. When evaluated according to Veber's rules, all synthesized compounds were found to comply with the established criteria. Taken together, these findings suggest that the synthesized compounds exhibit the physicochemical and structural characteristics necessary for drug-likeness and oral bioavailability, as summarized in Table 3. In terms of solubility, all compounds demonstrated favorable properties based on the SwissADME scale, which is a key factor in therapeutic absorption. Furthermore, the pharmacokinet-

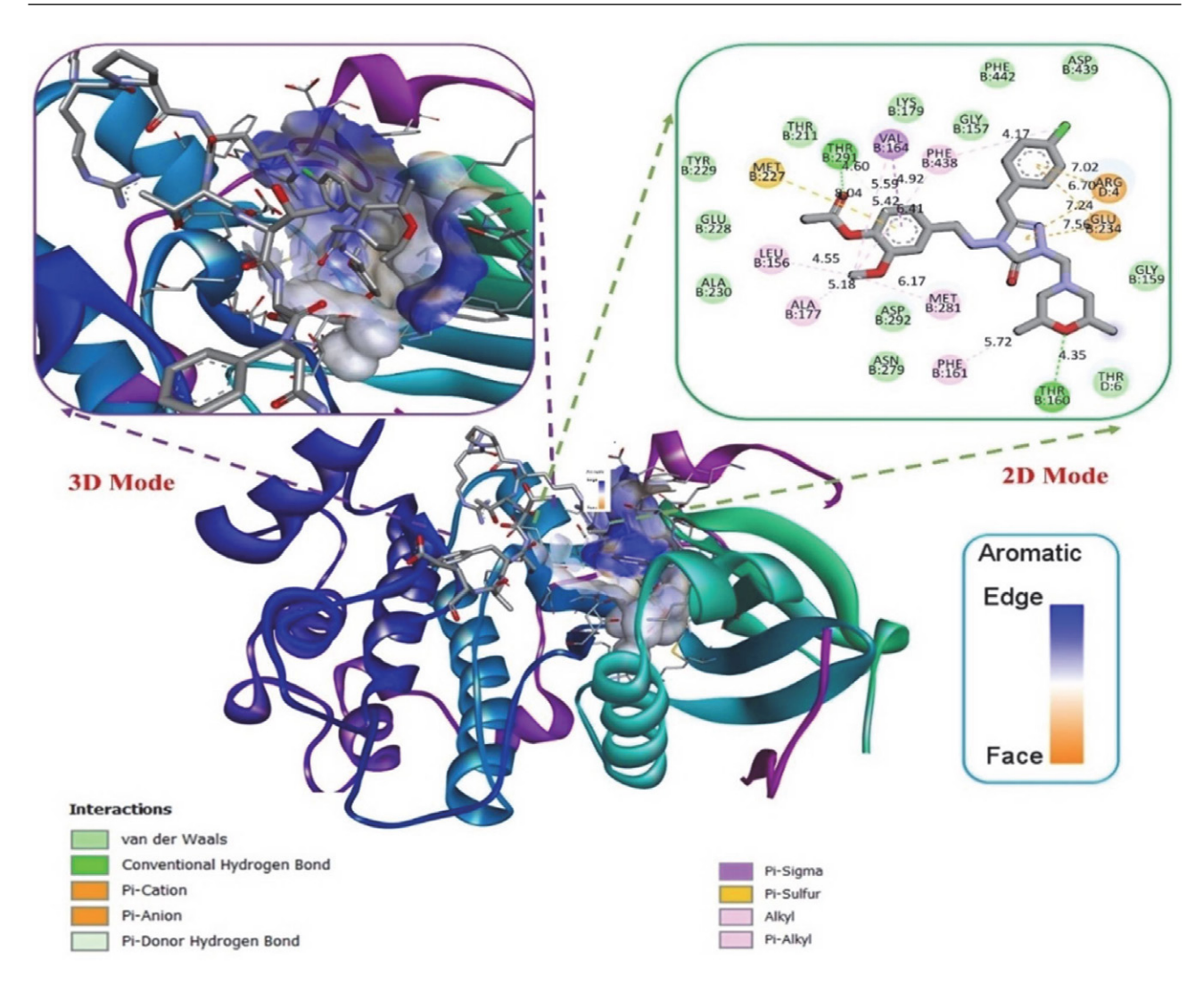


Figure 9. Interacts with 3OCB (Docking Score:-9.30) enzym of synthesized compound 6f; 3D view of the donor/acceptor surface of aromatic bonds on the receptor, 2D view of ligand-enzyme interactions

ic profiles of the compounds were analyzed using the Boiled-Egg model, as illustrated in Figure 10. This model assessed parameters such as blood-brain barrier (BBB) permeability, gastrointestinal (GI) absorption, skin penetration, and drug excretion. The results indicated that all synthesized compounds showed high gastrointestinal absorption but were not capable of crossing the blood-brain barrier. This lack of blood-brain barrier permeability is likely due to the relatively high topological polar surface area (TPSA) and the presence of multiple hydrogen bond donors and acceptors, which limit passive diffusion into the central nervous system. Skin permeability, another key pharmacokinetic property, was calculated based on the model developed by Potts and Guy. The corresponding values for the synthesized compounds are presented in Table 3. According to this model, skin permeability decreases as the negative Log Kp value increases. Figure 11 presents the molecular structures, color-coded physicochemical regions, and relevant parameters of the synthesized compounds. In the polar surface area (PSA) maps, the pink region represents the physicochemical space favorable for oral bioavailability. As shown in the bioavailability radar diagram, the compounds generally fall within this pink region, though slightly outside the saturation threshold. The positioning of the compounds within the pink zone of the

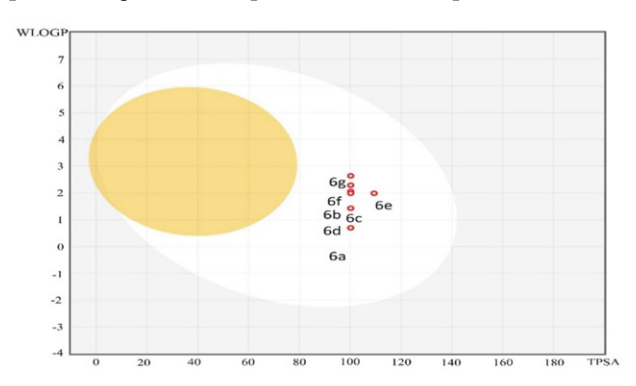


Figure 10: The Boiled-Egg model represents of the 6(a-g)

Table 3. The physicochemical and lipophilicity of the 6(a-g)

ADME Properties	6a	6b	6c Physic	6d ochemical-pro	6e opertie	6f	6g
Molecular weight (g/mol)	417.46	479.53	493.55	445.51	507.58	528.00	523.58
Heavy Atoms	30	35	36	32	37	37	38
Aromatic heavy atoms	11	17	17	11	17	17	17
Rotable bond	7	8	9	7	9	9	10
H acceptor bond	8	8	8	8	8	8	9
H donor bond	0	0	0	0	0	0	0
Molar refractivity	114.76	135.23	139.25	126.02	144.22	144.26	145.74
Absorption Percent	74.43	74.43	74.43	74.43	74.43	74.43	71.25
Topological Polar Surface Area (TPSA)	100.18	100.18	100.18	100.18	100.18	100.18	109.41
			Lipophilicit	y			
M LOGP	1.73	2.97	2.97	2.52	3.20	3.43	2.97
			Water solubil	ity			
LogS (ESOL)	-3.21	-4.66	-4.63	-4.13	-4.94	-5.23	-4.72
Solubility	Soluble	Mid-degree soluble	Mid-degree soluble	Mid-degree soluble	Mid-degree soluble	Mid-degree soluble	Mid-degree soluble
		F	harmacokine	etics			
Absorption	High	High	High	High	High	High	High
BBB permeant	No	No	No	No	No	No	No
Log Kp (skin permeation-cm/s)	-7.75	-6.95	-7.08	-7.07	-6.91	-6.85	-7.29
			Druglikenes	6 S			
Lipinski violation	Yes; 0	Yes; 0	Yes; 0	Yes; 0	Yes; 1	Yes; 1 violation:	No; 2 violations:
Ghose violation	Yes;	No;	No;	Yes;	No;	No;	No;
	0	1 violation	2 violations	0	2 violations:	2 violations:	3 violations:
Veber violation	Yes; 0	Yes; 0	Yes; 0	Yes; 0	Yes; 0	Yes; 0	Yes; 0
Bioavailability score	0.55	0.55	0.55	0.55	0.55	0.55	0.17

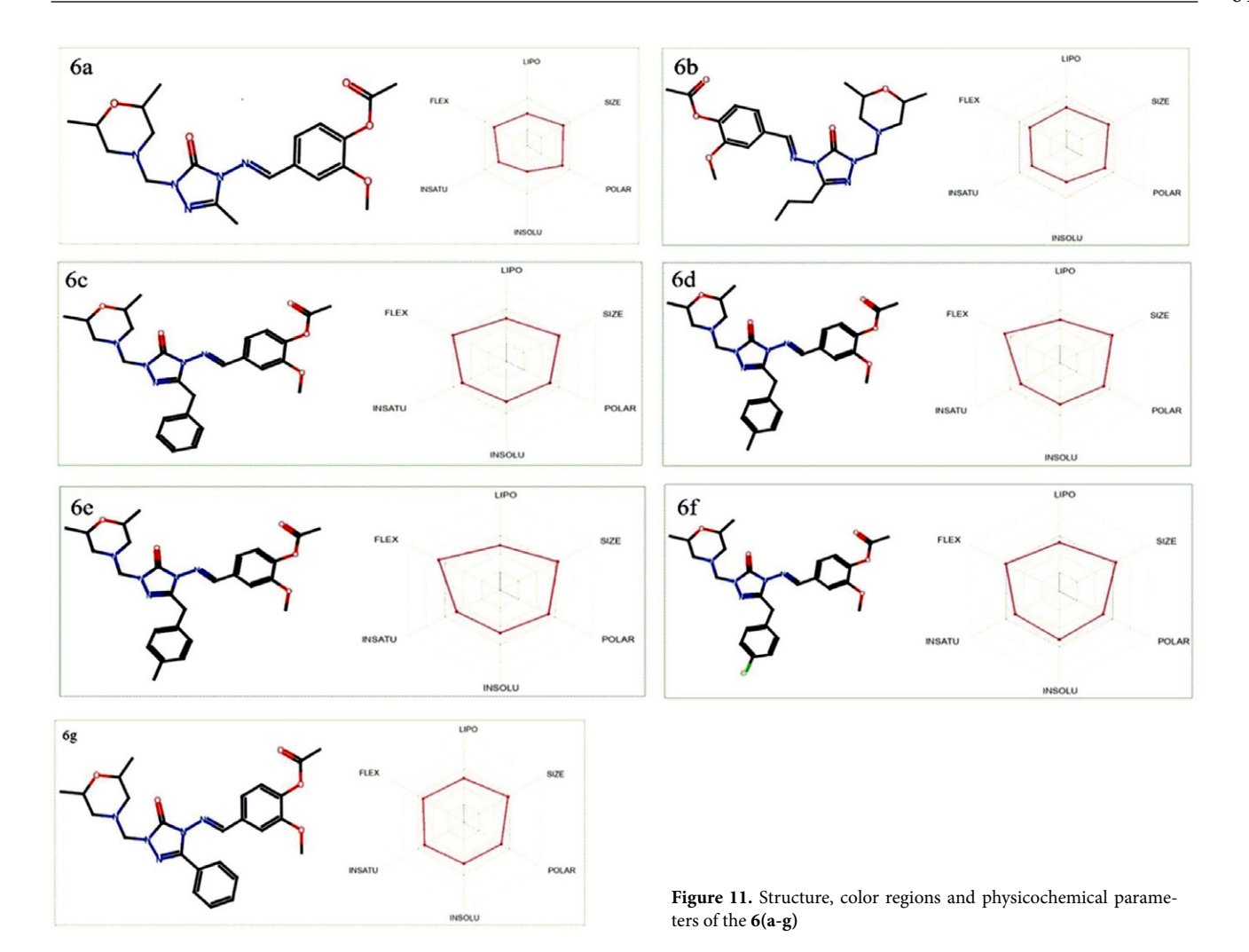
dABS%: absorption percent

radar plot supports their drug-likeness, as this region reflects the optimal range for key parameters such as lipophilicity, polarity, molecular size, and molecular flexibility-all of which contribute positively to oral bioavailability.

3. 3. 3. FMO's (Frontier Molecule Orbitals) Analysis

The highest occupied molecular orbital (HOMO) and the lowest unoccupied molecular orbital (LUMO) represent the frontier orbitals of a molecule. The energy gap between these orbitals (E_{LUMO}-E_{HOMO} difference) is a critical parameter for evaluating the electronic properties and chemical reactivity of the molecule.⁵⁷ This energy difference is directly related to key characteristics such as chemical reactivity, electrical conductivity, and optical behavior.⁵⁸ A large HOMO–LUMO gap generally indicates a more stable and less reactive molecule, whereas a smaller gap suggests higher reactivity and greater ease of electron donation or acceptance. The calculated HOMO–LUMO energy gap values and

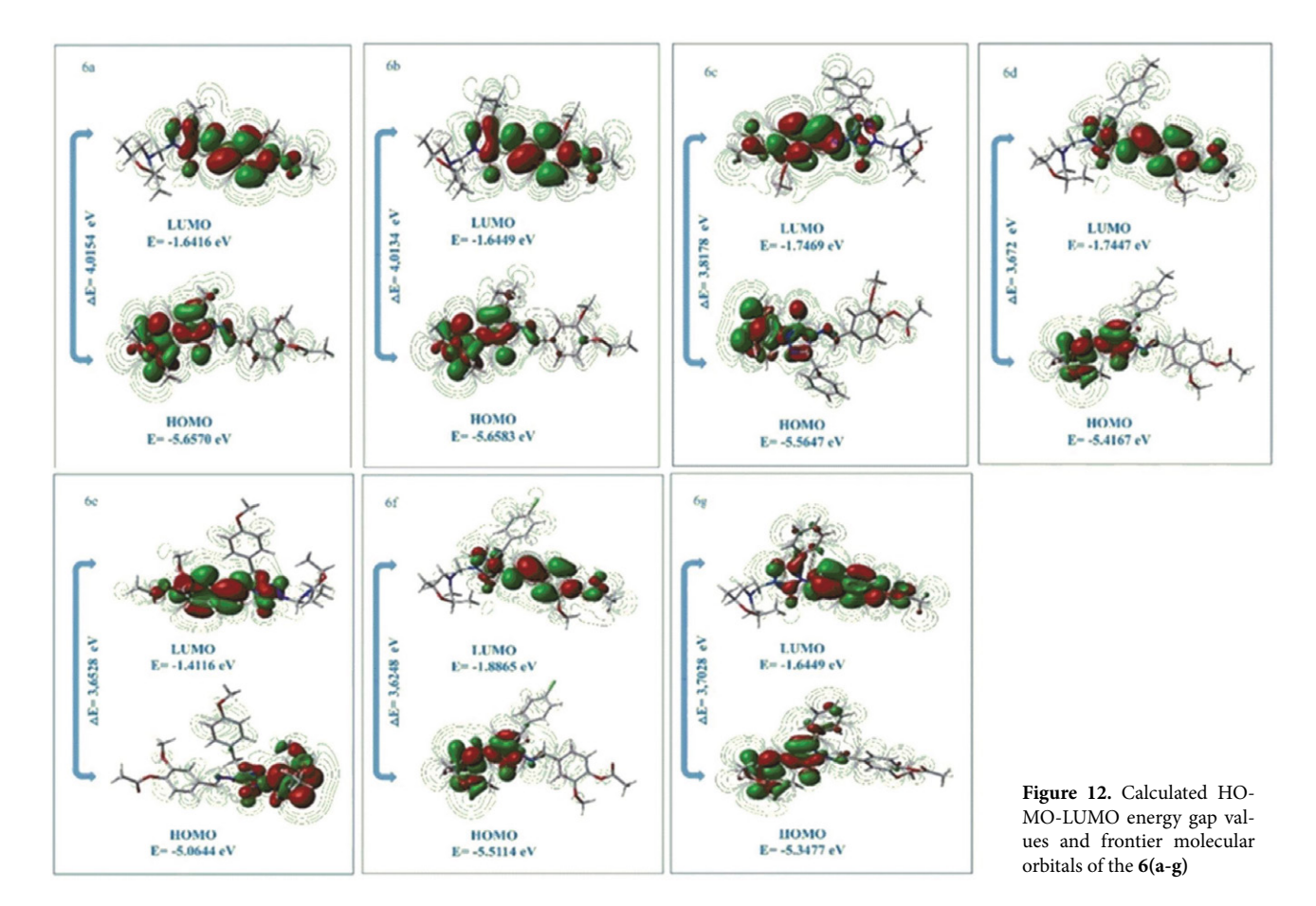
visual representations of the frontier molecular orbitals for the synthesized compounds have been provided in Figure 12. The Δ Eg values for compounds 6(a-g) were calculated as 4.01, 4.01, 3.81, 3.67, 3.65, 3.62, and 3.70 eV, respectively. Among these, compound **6f** exhibited the lowest energy gap (3.62 eV), indicating higher chemical reactivity compared to the others. The relatively small ΔEg value of compound 6fsuggests that it can readily participate in electron transfer processes. This increased reactivity of compound 6f can be attributed to the presence of a strong electron-donating group at a conjugated position, which raises the HOMO energy level and narrows the HOMO-LUMO gap. In contrast, compounds 6a and 6b, which exhibit the highest energy gaps (4.01 eV), contain relatively less conjugated or more electron-withdrawing substituents, resulting in lower HO-MO levels and therefore reduced reactivity. These observations indicate that the nature and position of the substituents on the aromatic ring play a critical role in modulating the frontier molecular orbital energies and, consequently, the chemical behavior of the compounds.



3. 3. 4. SAR Analysis

In biology and chemistry, structure activity relationships (SAR) are a fundamental concept, especially in drug discovery. SAR describes the relationship between a molecule's chemical structure and its biological activity, providing valuable insights for designing more potent and selective therapeutic agents. It examines how structural elements such as functional groups, ring systems, atomic arrangements, and other physicochemical features influence a molecule's effectiveness on its biological target.⁵⁹ Biological activity is typically evaluated based on the molecule's ability to interact with a specific target, such as enzyme inhibition, receptor activation, or modulation of other biological processes. SAR studies involve systematic modifications of molecular structures to assess how these changes affect biological responses.⁶⁰ This process helps identify which structural features enhance or diminish activity. Physicochemical Parameters: Key contributors to SAR include hydrogen bonding capacity, molecular volume, lipophilicity (log P), and polarity. Pharmacophore Models: These describe the essential three-dimensional

features of a molecule required to elicit a specific biological response.⁶¹ To investigate the structure-activity relationships of the synthesized compounds, correlations between their antibacterial activities and molecular characteristics were analyzed. Specifically, LUMO energy, molecular weight, total energy, and molecular volume were considered. Among these, LUMO and density were found to be closely associated with antibacterial activity. The LUMO (Lowest Unoccupied Molecular Orbital) level is a crucial parameter for evaluating a molecule's electrophilicity and reactivity. Molecules with low LUMO values are more reactive because they can more readily accept electrons. According to theoretical calculations, compound 6f had the lowest LUMO energy value (-1.886 eV), indicating high electrophilicity. In antibacterial applications, high LUMO reactivity can enhance interaction with the bacterial membrane. The compound may integrate more effectively into the lipophilic layer of the bacterial envelope, increasing membrane permeability and ultimately inhibiting bacterial growth. Density, another important parameter, reflects how closely packed a molecule's atoms are. It is calculated as the ratio of molecular weight to molecular volume. No-



tably, density is inversely proportional to molecular reactivity; compounds with lower densities tend to be more reactive. The calculated density values, along with mass and volume, are presented in Table 4. Among all synthesized compounds, compound **6f** had the lowest density (1.2198 g/cm³) and lowest LUMO energy (–1.886 eV), suggesting that it exhibits the highest antibacterial activity due to its superior reactivity.

4. Conclusion

In this study, seven novel Mannich base derivatives were synthesized and structurally characterized using 13 C

NMR, ¹H NMR, and IR spectroscopy techniques. The antioxidant activities of the synthesized compounds **6(a-g)** were evaluated *in vitro* using three different methods. While the compounds did not exhibit significant reducing power compared to standard antioxidants, they showed low levels of radical scavenging activity. On the other hand, due to the presence of C=O, -O-, and -NR₂ functional groups, high metal chelation activity was observed. The antimicrobial effects of the Mannich derivatives were tested against six different bacterial strains. The results indicated that the compounds did not show effects comparable to standard antibiotics. However, the highest antibacterial activity was observed against *Klebsiella pneumoniae* and *Escherichia coli*, while the weakest activity was seen

Table 4. Some parameters of 6(a-g) calculated using the DFT method

Compounds	Total Energy (a.u)	LUMO (eV)	Mol. Wt. (amu)	Volume (Å ³)	Density
6a	-1428.259636	-1.641	417.201	277.596	1.5029
6b	-1506.891910	-1.644	445.232	336.509	1.3111
6c	-1659.296693	-1.746	493.482	302.823	1.6296
6d	-1698.612351	-1.744	507.248	400.427	1.2492
6e	-1773.830499	-1.416	523.243	349.317	1.4979
6f	-2118.884017	-1.886	527.193	432.185	1.2198
6g	-1619.975061	-1.644	479.216	376.862	1.2715

against Pseudomonas aeruginosa. Among the 6(a-g) series, only compound 6a exhibited activity against all tested bacteria. To investigate the potential anticancer activities, in silico molecular docking studies were conducted against ovarian (PDB: 3W2S) and stomach (PDB: 3OCB) cancer target proteins. Among the synthesized compounds, 6e showed the strongest interaction with the 3W2S protein, with a docking score of -8.10, while 6f exhibited the highest binding affinity to the 3OCB protein, with a score of -9.30. Compared to reference and control ligands, these results suggest that compounds **6e** and **6f** possess promising anticancer potential. To further evaluate their potential as drug candidates, ADME (Absorption, Distribution, Metabolism, and Excretion) analyses were performed. All compounds complied with at least two of the five criteria defined by Lipinski, Veber, and Ghose rules, indicating good drug-likeness and suggesting their suitability as potential pharmaceutical agents. Additionally, HOMO-LU-MO energy levels and their energy gap (ΔE) were theoretically calculated. The compound **6f** showed the lowest ΔE value, indicating higher chemical reactivity compared to the others. This result is consistent with the compound's observed antimicrobial activity, SAR, favorable ADME profile, and molecular docking performance. Overall, compound 6f stands out as a promising multifunctional lead molecule with potential for further drug development.

Acknowledgments

This research did not receive any particular grant from funding sources in the public, private, or not-forprofit sectors.

5. References

- G. Kotan, S. Manap, H. Yüksek, J. Comput. Biophys. Chem. 2022, 21, 47–63. DOI:10.1142/S2737416522500041
- H. Medetalibeyoğlu, S. Manap, M. Alkan, M. Beytur, N. Barlak, O. F. Karatas, B. Tüzün, H. Yüksek, P. Taslimi, *Polycycl. Aromat. Compd.* 1–19.

DOI:10.1080/10406638.2024.2412217

- A. Hameed, M. al-Rashida, M. Uroos, S. Abid Ali, K. M. Khan, Expert Opin. Ther. Patents 2017, 27, 63–79.
 DOI:10.1080/13543776.2017.1252752
- 4. S.-S. Zhang, Q.-W. Tan, L.-P. Guan, *Mini-Rev. Med. Chem.* **2021**, *21*, 2261–2275.

DOI:10.2174/1389557521666210111145011

- M. Krátký, N.-H. Houngbedji, J. Vinšová, *Eur. J. Med. Chem.* 2024, 116835. DOI:10.1016/j.ejmech.2024.116835
- C. A. Ukwubile, E. O. Ikpefan, M. Y. Dibal, V. A. Umeano, D. N. Menkiti, C. C. Kaosi, S. Paul, A. C. Famurewa, H. Nettey, T. S. Yerima, *J. Ethnopharmacol.* 2023, 314, 116632.

DOI:10.1016/j.jep.2023.116632

7. C. Boulechfar, H. Ferkous, A. Delimi, A. Djedouani, A. Kahl-

- ouche, A. Boublia, A. S. Darwish, T. Lemaoui, R. Verma, Y. Benguerba, *Inorg. Chem. Commun.* **2023**, *150*, 110451. **DOI:**10.1016/j.inoche.2023.110451
- J. Ceramella, D. Iacopetta, A. Catalano, F. Cirillo, R. Lappano, M.S. Sinicropi, *Antibiotics* 2022, 11, 191.
 DOI:10.3390/antibiotics11020191
- M. Pervaiz, S. Sadiq, A. Sadiq, U. Younas, A. Ashraf, Z. Saeed, M. Zuber, A. Adnan, *Coord. Chem. Rev.* 2021, 447, 214128. DOI:10.1016/j.ccr.2021.214128
- M. Salihović, M. Pazalja, S. Špirtović Halilović, E. Veljović, I. Mahmutović-Dizdarević, S. Roca, I. Novaković, S. Trifunović, J. Mol. Struct. 2021, 1241, 130670.

DOI:10.1016/j.molstruc.2021.130670

11. J. Jorge, K. F. Del Pino Santos, F. Timóteo, R. R. Piva Vasconcelos, O. Ignacio Ayala Cáceres, I. Juliane Arantes Granja, D.M. de Souza, T. E. Allievi Frizon, G. Di Vaccari Botteselle, A. Luiz Braga, S. Saba, H.u. Rashid, J. Rafique, *Curr. Med. Chem.* 2024, 31, 2330–2344.

DOI:10.2174/0929867330666230224092830

C. Zalaru, F. Dumitrascu, C. Draghici, I. Tarcomnicu, M. Marinescu, G. M. Nitulescu, R. Tatia, L. Moldovan, M. Popa, M.C. Chifiriuc, *Antibiotics* 2022, 11, 1094.

DOI:10.3390/antibiotics11081094

- P. Guerra, M. Kim, A. Shah, M. Alaee, S. Smyth, *Sci. Total Environ.* 2014, 473, 235–243.
 DOI:10.1016/j.scitotenv.2013.12.008
- M. R. Aouad, *Molecules*. 2014, 19, 18897–18910.
 DOI:10.3390/molecules191118897
- S. Janowska, S. Andrzejczuk, P. Gawryś, M. Wujec, *Molecules* 2023, 28, 5562. DOI:10.3390/molecules28145562
- M. Y. Gvozdev, I. S. Turomsha, N. V. Loginova, E. Y. Varfolomeeva, R. A. Kovalev, N. D. Fedorova, G. A. Ksendzova, N. P. Osipovich & R. L. Sverdlov, *Free Radic. Res.* 2024, 58(11), 770-781. DOI:10.1080/10715762.2024.2433985
- Y. Guo, J. Fan, L. Qu, C. Bao, Q. Zhang, H. Dai, R. Yang, *Ind. Crop. Prod.* 2019, 141, 111762.

DOI:10.1016/j.indcrop.2019.111762

- F. Kardaş, Ö. Gürsoy-Kol, M. Beytur, M. Alkan, H. Yüksek, Int. Res. J. Pure Appl. Chem. 2017, 15, 1–9.
 DOI:10.9734/IRJPAC/2017/37845
- 19. Y. Ünver, S. Deniz, F. Çelik, Z. Akar, M. Küçük, K. Sancak, J. Enzyme Inhib. Med. Chem. **2016**, *31*, 89–95.

DOI:10.1080/14756366.2016.1206088

- B. B. Aggarwal, P. Gehlot, Curr. Opin. Pharmacol. 2009, 9, 351–369. DOI:10.1016/j.coph.2009.06.020
- 21. A. L. Coker, D. R. Follingstad, L. S. Garcia, H. M. Bush, *Cancer Causes Control* **2017**, *28*, 23–39.

DOI:10.1007/s10552-016-0833-3

- N. Bertoni, M. C. de Souza, S. Crocamo, M. Szklo, L.M. de Almeida, *Int. J. Behav. Med.* 2019, 26, 85–90.
 DOI:10.1007/s12529-018-9737-9
- G. C. Jayson, E. C. Kohn, H. C. Kitchener, J. A. Ledermann, The Lancet. 2014, 384, 1376–1388.

DOI:10.1016/S0140-6736(13)62146-7

A. Verdecchia, A. Mariotto, G. Gatta, M. T. Bustamante-Teixeira, W. Ajiki, Eur. J. Cancer. 2003, 39, 1603–1609.

- DOI:10.1016/S0959-8049(03)00360-5
- T. C. P. Dinis, V. M. C. Madeira, L. M. Almeida, *Arch. Biochem. Biophys.* 1994, 315, 161–169.
 DOI:10.1006/abbi.1994.1485
- 26. M. S. Blois, *Nature*, **1958**, *181*, 1199–1200. **DOI:**10.1038/1811199a0
- 27. M. Oyaizu, *Jpn. J. Nutr.* **1986**, *44*, 307–315. **DOI:**10.5264/eiyogakuzashi.44.307
- 28. I. B. Obot, D. D. Macdonald, Z. M. Gasem, *Corros. Sci.* **2015**, 99, 1–30. **DOI**:10.1016/j.corsci.2015.01.037
- A. P. S. Raman, M.B. Singh, M. Chaudhary, I. Bahdur, P. Jain,
 N. Kaushik, E. H. Choi, N. K. Kaushik, A. A. Lal, P. Singh, J.
 Mol. Liq. 2022, 362, 119650.
 - **DOI:**10.1016/j.molliq.2022.119650
- B. Khan, A. Naiyer, F. Athar, S. Ali, S. C. Thakur, J. Biomol. Struct. Dyn. 2021, 39, 457–475.
 - **DOI:**10.1080/07391102.2019.1711193
- 31. A. Pachuta-Stec, *Mini. Rev. Med. Chem.* **2022**, *22*, 1081–1094. **DOI:**10.2174/1389557521666210401091802
- D. Ünlüer, Y. Ünver, E. Düğdü, Y. B. Alpaslan, Y. Köysal, M. S. Soylu, K. Sancak, *Russ. J. Organ. Chem.* 2019, 55, 254–261.
 DOI:10.1134/S1070428019020192
- A. Harmankaya, Y. Yilmaz, S. Manap, H. Yuksek, O. Gursoy Kol, M. Alkan, EPSTEM. 2018, 72–80.
- G. Ö. Toraman, A. Bayrakdar, E. Oğuz, M. Beytur, F. Türkan, S. Manap, A. Aras, H. Yüksek, *J. Mol. Struct.* 2025, 1321, 139733. DOI:10.1016/j.molstruc.2024.139733
- 35. S. Release, 1: Maestro, Schrodinger, LLC, New York. 2019.
- A. Daina, O. Michielin, V. Zoete, *Sci. Rep.* 2017, *7*, 42717.
 DOI:10.1038/srep42717
- 37. G. W. T. M.J. Frisch, H. B. Schlegel, G. E. Scuseria, M.A. Robb, J. R. Cheeseman, G. Scalmani, V. Barone, B. Mennucci, G.A. Petersson, H. Nakatsuji, M. Caricato, X. Li, H. P. Hratchian, A. F. Izmaylov, J. Bloino, G. Zheng, J. L. Sonnenberg, M. Hada, M. Ehara, K. Toyota, R. Fukuda, J. Hasegawa, M. Ishida, T. Nakajima, Y. Honda, O. Kitao, H. Nakai, T. Vreven, J.A. Montgomery Jr., J.E. Peralta, F. Ogliaro, M. Bearpark, J. J. Heyd, E. Brothers, K. N. Kudin, V. N. Staroverov, R. Kobayashi, J. Normand, K. Raghavachari, A. Rendell, J. C. Burant, S. S. Iyengar, J. Tomasi, M. Cossi, N. Rega, J. M. Millam, M. Klene, J. E. Knox, J. B. Cross, V. Bakken, C. Adamo, J. Jaramillo, R. Gomperts, R. E. Stratmann, O. Yazyev, A. J. Austin, R. Cammi, C. Pomelli, J. W. Ochterski, R. L. Martin, K. Morokuma, V.G. Zakrzewski, G. A. Voth, P. Salvador, J. J. Dannenberg, S. Dapprich, A. D. Daniels, Ö. Farkas, J. B. Foresman, J. V. Ortiz, J. Cioslowski, D. J. Fox, Gaussian 09. 2009.
- 38. Ö. Gürsoy Kol, Fen Bilimleri Enstitüsü, Doktora Tezi, 393s, Kars, 2008.
- H. Yüksek, E. Koca, Ö. Gürsoy-Kol, O. Akyıldırım, M. Çelebier, *J. Mol. Liq.* 2015, 206, 359–366.
 DOI:10.1016/j.molliq.2015.02.038
- 40. I. Shahzadi, M. Islam, H. Saeed, A. Shahzadi, J. Haider, A. Haider, M. Imran, H. A. Rathore, A. Ul-Hamid, W. Nabgan, M. Ikram, *Int. J. Biol. Macromol.* 2023, 235, 123874. DOI:10.1016/j.ijbiomac.2023.123874
- 41. O. Aktas-Yokus, H. Yuksek, O. Gursoy-Kol, S. Alpay-Karao-

- glu, Med. Chem. Res. **2015**, *24*, 2813–2824. **DOI:**10.1007/s00044-015-1334-8
- K. Gören, G. Kotan, S. Manap, H. Yüksek, Chem. Afr. 2024, DOI:10.1007/s42250-024-01139-2
- 43. M. Balouiri, M. Sadiki, S. K. Ibnsouda, *J. Pharm. Analys.* **2016**, *6*, 71–79. **DOI:**10.1016/j.jpha.2015.11.005
- 44. N. Ye, Z. Yang, Y. Liu, *Drug Discov. Today.* **2022**, *27*, 1411–1419. **DOI**:10.1016/j.drudis.2021.12.017
- 45. F. Basha, F. L. A. Khan, S. Muthu, M. Raja, *Chem. Data Coll.* **2021**, *31*, 100609. **DOI**:10.1016/j.cdc.2020.100609
- 46. K. H. Lee, J. Y. Lee, Y. G. Hwang, *Bull. Korean Chem. Soc.* **2013**, *34*, 365–366. **DOI:**10.5012/bkcs.2013.34.2.365
- G. Kotan, Lett. Org. Chem. 2021, 18, 830–841.
 DOI:10.2174/1570178617999201216113719
- S. Manap, H. Medetalibeyoğlu, A. Kılıç, O. F. Karataş, B. Tüzün, M. Alkan, A. B. Ortaakarsu, A. Atalay, M. Beytur, H. Yüksek, *J. Biomol. Struct. Dyn.* 2024, 42, 11916-11930.
 DOI:10.1080/07391102.2023.2265501
- S. Boy, A. Aras, F. Türkan, O. Akyıldırım, M. Beytur, H. Sedef Karaman, S. Manap, H. Yüksek, *Chem. Biodivers.* **2021**, *18*, e2100433. **DOI:**10.1002/cbdv.202100433
- S. Dutta, P. S. Kharkar, N. U. Sahu, A. Khanna, *Life Sci.* 2017, 185, 73–84. DOI:10.1016/j.lfs.2017.07.015
- H. Medetalibeyoğlu, F. Türkan, S. Manap, E. Bursal, M. Beytur, A. Aras, O. Akyıldırım, G. Kotan, Ö. Gürsoy-Kol, H. Yüksek, *J. Biomol. Struct. Dyn.* 2023, 41, 4286–4294.
 DOI:10.1080/07391102.2022.2066021
- O. Akyıldırım, H. Medetalibeyoğlu, E. Oğuz, A. Aras, A. Atalay, A. Korkmaz, M. Beytur, F. Türkan, H. Yüksek, *Mol. Struct.* 2023, *1293*, 136321. DOI:10.1016/j.molstruc.2023.136321
- 53. S. K. Burley, H. M. Berman, C. Bhikadiya, C. Bi, L. Chen, L. Di Costanzo, C. Christie, K. Dalenberg, J. M. Duarte, S. Dutta, Z. Feng, S. Ghosh, D. S. Goodsell, R. K. Green, V. Guranović, D. Guzenko, B. P. Hudson, T. Kalro, Y. Liang, R. Lowe, H. Namkoong, E. Peisach, I. Periskova, A. Prlić, C. Randle, A. Rose, P. Rose, R. Sala, M. Sekharan, C. Shao, L. Tan, Y.-P. Tao, Y. Valasatava, M. Voigt, J. Westbrook, J. Woo, H. Yang, J. Young, M. Zhuravleva, C. Zardecki, Nucleic Acids Res. 2018, 47, D464–D474. DOI:10.1093/nar/gky1004
- 54. M. H. Abdellattif, A. Elkamhawy, M. Hagar, T. B. Hadda, W. S. Shehab, W. Mansy, A. Belal, M. Arief, M. A. Hussien, Front. Pharmacol. 2022, 13, 958379.
 - DOI:10.3389/fphar.2022.958379

DOI:10.1016/j.ejmech.2016.09.023

- H. Perumalsamy, K. Sankarapandian, K. Veerappan, S. Natarajan, N. Kandaswamy, L. Thangavelu, S.R. Balusamy, Phytomedicine. 2018, 46, 119-130.
 DOI:10.1016/j.phymed.2018.04.021
- 56. SwissADME. 2024,cited 2024.
- 57. V. Choudhary, A. Bhatt, D. Dash, N. Sharma, *J. Comput. Chem.* **2019**, 40, 2354–2363. **DOI:**10.1002/jcc.26012
- M. A. Mumit, T. K. Pal, M. A. Alam, M. A. Islam, S. Paul, M. C. Sheikh, *J. Mol. Struct.* 2020, 1220, 128715.
 DOI:10.1016/j.molstruc.2020.128715
- J. Akhtar, A. A. Khan, Z. Ali, R. Haider, M. S. Yar, Eur. J. Med. Chem. 2017, 125, 143–189.

G. Yadav, S. Ganguly, Eur. J. Med. Chem. 2015, 97, 419–443.
 DOI:10.1016/j.ejmech.2014.11.053

H. Liu, S. Long, K. Rakesh, G.-F. Zha, Eur. J. Med. Chem.
 2020, 185, 111804. DOI:10.1016/j.ejmech.2019.111804

Povzetek

V predstavljeni raziskavi so sintetizirali Mannichove bazne derivate 1-(2,6-dimetilmorfolin-4-il-metil)-3-alk-il(aril)-4-(3-metoksi-4-acetoksibenzilidenamino)-4,5-dihidro-1H-1,2,4-triazol-5-on 6(a-g). Strukture novih spojin so potrdili s pomočjo spektroskopskih metod, in sicer 1H NMR, ^{13}C NMR ter IR spektrometrijo. Potencialno antioksidativno delovanje spojin so ovrednotili s tremi uveljavljenimi metodami (Blois, Oyaizu, Dinis), medtem ko so njihove *in vitro* protibakterijske lastnosti preverili z metodo difuzije v agarju na šestih bakterijskih sevih. Dodatno so izvedli molekulsko sidranje, da bi raziskali potencialno protitumorno aktivnost spojin proti raku jajčnikov in želodca. Rezultati so pokazali, da je spojina 6e izkazala ugodne interakcije s proteinom 3W2S, spojina 6f pa s proteinom 3OCB. Opravljene so bile tudi ADME napovedi za vrednotenje podobnosti spojin z zdravilnimi učinkovinami. Izračunali so energije molekulskih orbital (HOMO–LUMO) ter energijske razlike (ΔEg). Nazadnje so razmerja med strukturo in delovanjem (SAR) analizirali s pomočjo teorije gostotonih funkcionalov (DFT).



Except when otherwise noted, articles in this journal are published under the terms and conditions of the Creative Commons Attribution 4.0 International License